Journal of Industrial and Engineering Chemistry 65 (2018) 411–417

Contents lists available at ScienceDirect

Journal of Industrial and Engineering Chemistry

journal homepage: www.elsevier.com/locate/jiec

The Vis-NIR multicolor emitting phosphor $Ba_4Gd_3Na_3(PO_4)_6F_2$: Eu^{2+}, Pr^{3+} for LED towards plant growth

Ziwei Zhou[a], Niumiao Zhang[a], Jiayu Chen[a], Xianju Zhou[b], Maxim S. Molokeev[c,d,e,**], Chongfeng Guo[a,*]

[a] National Key Laboratory of Photoelectric Technology and Functional Materials (Culture Base) in Shaanxi Province, National Photoelectric Technology and Functional Materials & Application of Science and Technology International Cooperation Base, Institute of Photonics & Photon-Technology and Department of Physics, Northwest University, Xi'an 710069, China
[b] School of Science, Chongqing University of Posts and Telecommunications, Chongqing, 400065, PR China
[c] Laboratory of Crystal Physics, Kirensky Institute of Physics, Federal Research Center KSC SB RAS, Krasnoyarsk, 660036, Russia
[d] Siberian Federal University, Krasnoyarsk, 660041, Russia
[e] Department of Physics, Far Eastern State Transport University, Khabarovsk, 680021, Russia

ARTICLE INFO

Article history:
Received 9 March 2018
Received in revised form 10 May 2018
Accepted 12 May 2018
Available online 21 May 2018

Keywords:
Phosphor
Plant growth
LEDs
Energy-transfer

ABSTRACT

Photosynthesis process is the basic for plant growth, *which* needs energy from the light. The pigments of chlorophyll a, b and bacteriochlorophyll are responsible for the absorption of light, in which blue, red and near-infrared (NIR) light directly or indirectly promote the plant growth and enhancement of nurtiments. It is important for plant to support absorbable light, and phosphhor-converted light emitting diodes (pc-LEDs) are low-cost, energy-saving and enviromental friendly devices for plant growth. To develop a phosphor with emission covering the blue, red and NIR, a series of phosphors $Ba_4Gd_3Na_3(PO_4)_6F_2$: Eu^{2+}, Pr^{3+} with blue, red and NIR multi-emitting were prepared. Their emissions not only match well with the absorption spectra of pigments in the plant, but also could be excited by near ultraviolet (n-UV) LED chip. The crystal structure of host $Ba_4Gd_3Na_3(PO_4)_6F_2$ was refined from the XRD data and three different crystallographic sites occupied by Eu^{2+} were determined through low temperature photoluminescence spectra. The energy transfer from Eu^{2+} to Pr^{3+} ions was also discussed in detail. Results indicated that the multi-emitting $Ba_4Gd_3Na_3(PO_4)_6F_2$: Eu^{2+}, Pr^{3+} can serve as a phosphor candidate for plant growth LEDs.

Introduction

Light guides the growth rhythm and process of plants, and the spectral composition of light environment plays a crucial role. During the typical photosynthetic process, the pigments carotenoids and chlorophylls absorb blue (400–500 nm) and red (620–690 nm) light, which directly accelerate the photosynthetic action [1–3]. However, the role of near-infrared (NIR, 715–1050 nm) light could not be omitted since it could be efficiently absorbed by bacteriochlorophyll to convert chemical energy through anaerobic photosynthesis, which promote the reproduction of photosynthetic bacteria and indirectly motivate plant growth and development [4]. It is an efficient method to improve crop yields and quality and tune the growth cycle of plant through synergistic effect of blue, red and NIR, which could be realized by appropriate adjusting the components of artificial supplying illumination source. It is more useful and necessary in a short growing season or high latitude area with poor light [5,6]. The commonly used incandescent and fluorescent lamps for plant illumination suffer not only spectral mismatch, but also high energy consumption or environmental threat, whereas light-emitting diodes (LEDs) plant growth lights can overcome these shortcomings due to their high efficiency, long lifetime, environment friendly and controllable spectra composition advantages. Thus, LEDs are recognized as the first light source for plant photoreceptors to affect plant morphology and offer optimized production [7,8].

Phosphor-converted LEDs (pc-LEDs) are the dominant products in the market due to their low cost and mature fabrication approach, which are generally fabricated by combining LED chip and phosphors [9]. Their tunable spectral components strongly depend on phosphor selection, thus it is urgent to design and develop a phosphor with matched spectrum with plant growth.

* Corresponding author.
** Corresponding author at: Laboratory of Crystal Physics, Kirensky Institute of Physics, Federal Research Center KSC SB RAS, Krasnoyarsk 660036, Russia
E-mail addresses: msmolokeev@mail.ru (M.S. Molokeev), guocf@nwu.edu.cn (C. Guo).

https://doi.org/10.1016/j.jiec.2018.05.014
1226-086X/

Generally, several single color emission phosphors those can be excited efficiently by UV light have to be arranged in this scheme, leading to high cost and low luminous efficiency due to the complicated manufacture, reabsorption of emission colors and different aging rates for each phosphor. It is possible to improve the efficiency and decrease the cost of LEDs plant growth lamp through the application of a single phased multi-color-emitting phosphor with high chemical and thermal stability for UV-pumped LED plant growth illumination source [10].

As a typical dopant with broad excitation and emission, Eu^{2+} ions are popular activators for LED phosphors with changeable emission wavelength from near ultraviolet to near infrared due to the $4f^7 \rightarrow 4f^6 5d^1$ dipole allowed transition [11–14]. Because the d-shell electrons are easily influenced by surrounding crystal-field environments, the emission wavelength of Eu^{2+} ions strongly depends on the crystal field strength in the occupied sites of hosts. Apatites with the general formula $A_{10}(MO_4)_6X_2$ are important phosphor hosts, where A is the bivalent cation (Ca^{2+}, Ba^{2+}, Sr^{2+}, Mg^{2+}, and Pb^{2+}) or a trivalent RE^{3+} ion matching with a Na^+/K^+ ion; M is the small-size cation (P^{5+}, Si^{4+}, Ge^{4+}, and V^{5+}); and X represents anions O^{2-}, F^-, and Cl^-. A^{2+} ions are settled in two crystallographic sites: A (1) has 9-fold coordinated 4f site with C_3 symmetry, and A (2) has 7-fold coordinated 6 h site with C_s symmetry (seven O atoms and two F atoms, exactly) [15]. As a member of apatite family, $Ba_4Gd_3Na_3(PO_4)_6F_2$ (BGNPF): Eu^{2+} shows intense warm-white emissions centered at 485 and 570 nm under the n-UV excitation [16], which overlaps the excitation of the Pr^{3+} ion. The efficient energy transfer from Eu^{2+} ions to Pr^{3+} ions could be occurred, and the emission of Pr^{3+} covers blue ($^3P_0 \rightarrow {}^3H_4$), red ($^1D_2 \rightarrow {}^3H_4$) and NIR ($^1G_4 \rightarrow {}^3H_4$) from the spin-forbidden *f–f* transitions. It is possible to obtain a single-compound phosphor with multi-band emission by co-doping Eu^{2+} ion and Pr^{3+} ion in BGNPF host [17]. Thus, in the present study, the Eu^{2+} and Pr^{3+} ions co-doped BGNPF phosphors were synthesized via traditional high-temperature solid-state method to obtain a phosphor with blue-yellow and NIR multicolor emission. The crystallographic site occupancy by Eu^{2+} and Pr^{3+} ions, the photoluminescence and the energy transfer from Eu^{2+} to Pr^{3+} ions were investigated in detail in this contribution, which indicated that the obtain solid solution can serve as a potential phosphor for plant growth LEDs.

Experimental section

Materials and synthesis

Eu^{2+} and Pr^{3+} singly or co-doped $Ba_4Gd_3Na_3(PO_4)_6F_2$ (BGNPF) samples were prepared by a traditional high-temperature solid-state method, in which the stoichiometric amount of analytical reagent (A. R.) raw materials $BaCO_3$, Na_2CO_3, $NH_4H_2PO_4$, BaF_2 from Sinopharm Chemical Reagent Co., Ltd. and high purity Gd_2O_3 (99.99%), Eu_2O_3 (99.99%) and Pr_6O_{11} (99.99%) from Guangdong Zhujiang Rare Earth Co. Ltd. were first weighted and then mixed with an alcohol in evaporating dish. After that, the dish with raw materials was transferred into an oven to dry the mixture at 70 °C for 2 h and then thoroughly ground the powder for 20 min in an agate mortar. Then powder mixtures were pre-heated in furnace at 500 °C for 5 h, and subsequently sintered at 1075 °C for 6 h in CO reducing atmosphere to get the final samples.

Characterization and calculation

The powder X-ray diffraction (XRD) data of $Ba_4Gd_3Na_3(PO_4)_6F_2$ for Rietveld analysis were collected at room temperature with a Bruker D8 ADVANCE powder diffractometer (Cu-Kα radiation) and linear VANTEC detector. The step size of 2θ was 0.016°, and the counting time was 2 s per step. Rietveld refinement was performed by using TOPAS 4.2 [18]. The photoluminescence emission (PL) and excitation (PLE) spectra of phosphors as well as decay curves were measured on an Edinburgh FLS920 fluorescence spectrophotometer (Edinburgh Instruments Ltd., UK) equipped with a 450W Xe lamp and EPL-375 picosecond pulsed diode laser (Edinburgh Instruments Ltd.) as excitation sources. An oxford OptistatDN2 nitrogen cryogenics temperature controlling system was combined with spectrophotometer to measure the temperature-dependent PL spectra and duration of staying at the selected temperature was 10 min.

Results and discussion

The phase purity and crystal structure

The XRD pattern of blank phosphor BGNPF is shown in Fig. 1a, it is found that almost all diffraction peaks are indexed to trigonal cell (*P*-3) with parameters close to $Ba_4Nd_3Na_3(PO_4)_6F_2$ [19] (apatite-type structure, JCPDS# 71-1318) except few peaks from trace impurity $Na_3Gd(PO_4)_2$ (wt. = 5.9(4)%, as shown in the inset of Fig. 1a). Therefore, the crystal structure of $Ba_4Nd_3Na_3(PO_4)_6F_2$ is taken as initial model for Rietveld refinement under the supposition that the Nd ion sites are occupied by Gd ions. The refinement is stable with low R-factors (shown in Table 1). The cell parameters of hexagonal fluorophosphate BGNPF with space group *p*-3 are $a = b = 9.7477(3)$ and $c = 7.2220(3)$ Å, $V = 594.27(4)$ Å^3. The crystal structure of BGNPF accorded to refinement result is shown in Fig. 1b. There are one Ba^{2+} site and two Gd^{3+} cationic crystallographic sites in BGNPF. The coordination polyhedrons of Ba and Gd (1) are coordinated by seven oxygens and two fluorides, and the coordination number (CN) is 9. Gd (2) is coordinated by nine oxygens, which indicates that three cationic sites offer different crystal field environment for Eu^{2+} ions. Considering the similar ionic radii of dopant Eu^{2+} (r = 1.30 Å, CN = 9), Pr^{3+} (r = 1.319 Å, CN = 9) and cationic ions Ba^{2+} (r = 1.47 Å, CN = 9) or Gd^{3+} (r = 1.247 Å, CN = 9) in host, it is possible for Eu^{2+} and Pr^{3+} ions to randomly enter the sites of Ba^{2+} and Gd^{3+} [16].

The photoluminescent property of BGNPF: Eu^{2+} phosphor

The emission wavelength of Eu^{2+} strongly depends on the crystal field environment of the occupied sites because its typical $5d \rightarrow 4f$ transition. To identify the occupancy of Eu^{2+} in host $Ba_4Nd_3Na_3(PO_4)_6F_2$, the emission and excitation spectra of BGNPF: Eu^{2+} were recorded at liquid helium temperature (LHT) and they are shown in Fig. 2a. Under the excitation by 365 nm n-UV light, it is observed that the PL spectrum consists of a broad asymmetric emission band covering the region of 400–800 nm from the transition of Eu^{2+} $4f^6 5d^1 \rightarrow 4f^7$ along with a small sharp peak at 615 nm from the $^5D_0 \rightarrow {}^7F_2$ transition of unreduced Eu^{3+}. The former can be decomposed into three Gaussian peaks centered at 446, 484, and 593 nm, which imply that Eu^{2+} ions occupy three different sites. According to the structure analysis results, there are three cationic sites Ba, Gd (1), and Gd (2) that can be occupied by Eu^{2+} ions in the BGNPF host. For the same nine-coordination environment, the average bond length Ba/Gd (1)-O (~2.726 Å) (7O, 2F) is distinctly longer than that of Gd (2)-O (~2.453 Å) (9O), which means that the crystal field strength of Ba/Gd (1) site is weaker than that of Gd (2) site [20]. Thus, the emission band centered at 593 nm is assigned to Eu^{2+} ions located at Gd (2) site with stronger crystal field; whereas the emission of Eu^{2+} occupied the Ba site must be close to that of Gd (1) site due to their similar coordination environments. On the basis of previous discussion by Van Uitert [21,22], the

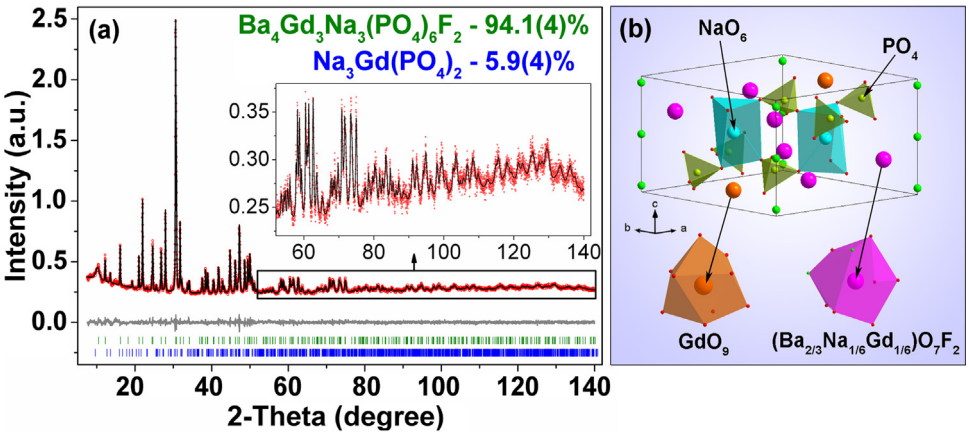

Fig. 1. (a) Difference Rietveld plot of $Ba_4Gd_3Na_3(PO_4)_6F_2$ with small amount of $Na_3Gd(PO_4)_2$ impurity; (b) crystal structure of $Ba_4Gd_3Na_3(PO_4)_6F_2$.

Table 1
Main parameters of processing and refinement of the $Ba_4Gd_3Na_3(PO_4)_6F_2$ sample.

Compound	$Ba_4Gd_3Na_3(PO_4)_6F_2$
Sp. Gr.	*P*-3
a, Å	9.7477 (3)
c, Å	7.2220 (3)
V, Å^3	594.27 (4)
Z	1
R_{wp}, %	2.67
R_p, %	2.05

environment-dependent emission position of Eu^{2+} ions can be evaluated by following equation [23]:

$$E = Q\left[1 - \left(\frac{V}{4}\right)^{\frac{1}{V}} \times 10^{-nE_a r/80}\right] \quad (3)$$

where E is the position of the *d*-band edge in energy for Eu^{2+} ion (cm^{-1}), Q is the position of the *d*-band edge in energy for free ion (Q = 34,000 for Eu^{2+}), V is the valence of the activator (V = 2 for Eu^{2+}), n is the coordination number of activator, r is the ion radii of the occupied cation by activator in the host, E_a is a constant for the same host and it is defined to be 1 by us to simplify the operation. In light of Eq. (3), E(Gd (1)) = 17,572.78 > 15,950.55 = E(Ba), which means the emission components centered at 446 and 484 nm should be attributed to entered the sites of Ba and Gd (1), respectively [24]. In sum up, the three emission bands at 446, 484 and 593 nm are assigned to activators Eu^{2+} occupied the sites of Ba, Gd (1) (coordinated with 7O and 2F) and Gd (2) site (coordinated with 9O), respectively. For the PLE spectra of BGNPF: Eu^{2+} at LHT monitored at 446, 484 and 593 nm, clear difference was observed between typical intense absorption broad bands from 250 to 450 nm assigned to the $4f^7 \rightarrow 4f^65d^1$ transition of Eu^{2+} [25]. The sharp line absorption peaks belonging to the $^7F_0 \rightarrow {}^5D_4$, $^5L_7$, $^5L_6$ transitions of Eu^{3+} were found in the PLE spectra monitored at 484 and 593 nm, whereas no sharp peaks were detected in the PLE spectrum monitored at 446 nm, which further indicate that it is difficult to reduce completely Eu^{3+} occupied the Gd^{3+} site to Eu^{2+} owing to the valence state imbalance.

By contrast, the sharp line emission for the unreduced Eu^{3+} disappeared and the dominant emission band obviously shifts to blue region in the PL spectra of BGNPF: Eu^{2+} at room temperature (in Fig. 2b). However, it could overlap with the absorption of carotenoid, chlorophyll a and b with the excitation of 365 nm near ultraviolet light, which indicated the prepared phosphors BGNPF: Eu^{2+} could be used in the plant growth LEDs. To determine the optimal composition of the phosphor, the PL profiles of BGNPF: xEu^{2+} were presented in Fig. 2c as a function of Eu^{2+} concentration under the excitation of 340 nm. It is observed that the PL intensity first gradually increases and then declines after reaching the maximum value at x = 0.9% due to the concentration quenching resulting from the shorter and shorter distance between identical Eu^{2+} ions in the crystal host. The critical distance (R_c) can be estimated by the following formula [26]:

$$R_c = 2\left[\frac{3V}{4\pi x_c N}\right]^{1/3} \quad (1)$$

where V is the volume of the unit cell, N is the number of host cations in the unit cell, and x_c is the critical concentration of Eu^{2+} ions. The calculated critical distance (R_c) is about 26.21 Å according to the V = 594.27(4) Å^3, N = 7, and x_c = 0.009, which is far beyond 5 Å that means the energy transfer among Eu^{2+} ions is not controlled by exchange interaction mechanism which generally occurred in a forbidden transition. Moreover, the inapparent overlap between the excitation and emission spectra hints that the electric multipolar interaction energy transfer is responsible for the concentration quenching, and the type of interaction can be described by following equation [27,28]:

$$\frac{I}{x} = K\left[\frac{1}{1+\beta(x)^{\theta/3}}\right] \quad (2)$$

where I is the PL intensity, x is the activator concentration over the critical concentration, K and β are constants for the same excitation condition and host lattice. The values of θ = 3, 6, 8, or 10 are representative for the non-radiative energy transfer mechanism of exchange coupling, namely, dipole–dipole (d–d), dipole–quadrupole (d–q), and quadrupole–quadrupole (q–q) interactions, respectively. The slop of well-fitted straight line on the basis of Ln(I/x) *vs* Ln(x) is −1.55 (−θ/3), as shown in Fig. 2d. The value of θ is calculated to be 4.65 that is between 3 and 6, which indicates that the exchange coupling and d–d interaction mechanism collectively dominate the concentration quenching effect in BGNPF: Eu^{2+}.

For the practical application of phosphor in LEDs, its thermal stability is a vital parameter owing to about 150 °C operating temperature of LED chip [10]. The intensity map of temperature-dependent PL spectra of BGNPF: 0.9%Eu^{2+} phosphor with optimal composition is displayed in Fig. 3a, and it is found that the emission intensity decreases gradually with temperature increase. Meanwhile, the descent speed of PL intensity in yellow region is faster than that in blue region, which further proves that yellow and blue emissions come from different luminescence centers related to Eu^{2+} in different cationic sites. The normalized integrated intensities (400–800 nm) of

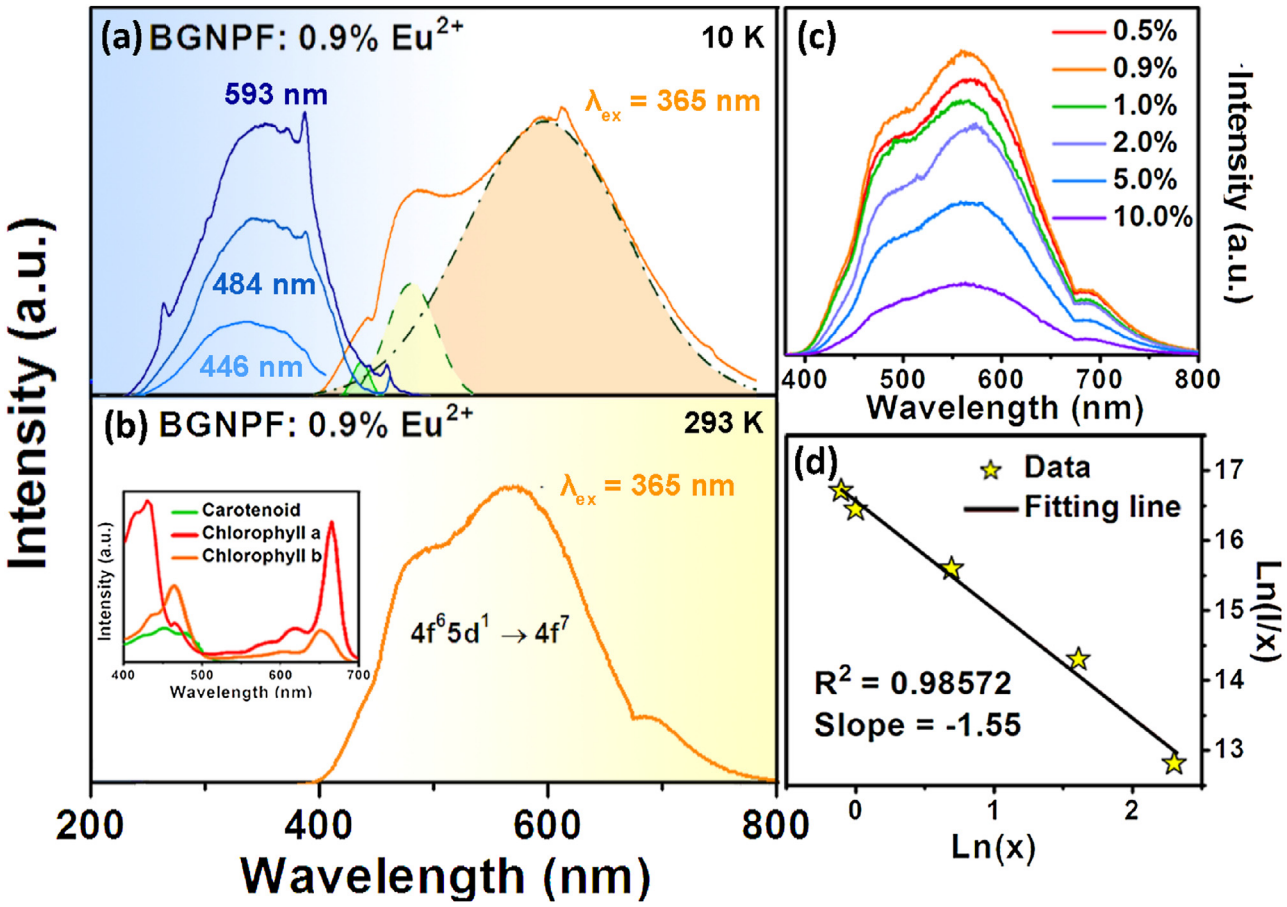

Fig. 2. (a) The PLE (λ_{em} = 446, 484, 593 nm) and PL (λ_{ex} = 365 nm) spectra of BGNPF: Eu^{2+} at 10 K and (b) the PL spectra of BGNPF: Eu^{2+} at room temperature; (c) the Eu^{2+} contents-dependent PL spectra of BGNPF: xEu^{2+} (x = 0.5%–10.0%) and (d) the dependence of ln(I/x) on ln(x). The inset of (b) is the absorb spectra of carotenoid, chlorophyll a and b.

BGNPF: 0.9%Eu^{2+} was also given in Fig. 3b as a function of heating temperature from 298 to 498 K. The integrated PL intensity decreases with increasing temperature and reaches about 37.3% of the initial intensity at 423 K. The thermal activation energy ΔE_a can be calculated according to following equation [29]:

$$I(T) = \frac{I(0)}{1 + cexp(-\Delta E_a/k_B T)} \quad (4)$$

where $I(0)$ is the initial emission intensity at room temperature, $I(T)$ is the emission intensity at temperature T, c is a constant, ΔE_a is thermal activation energy, K is the Boltzmann constant (K = 8.62 × 10^{-5} eV). The experimental data are well fitted by the plot of ln($I_0/I - 1$) *vs* 10,000/T, as shown in Fig. 3c, and the thermal activation energy ΔE_a is calculated to be 0.29 eV. Furthermore, it is noteworthy that the blue emission peak (485 nm) shows a slight

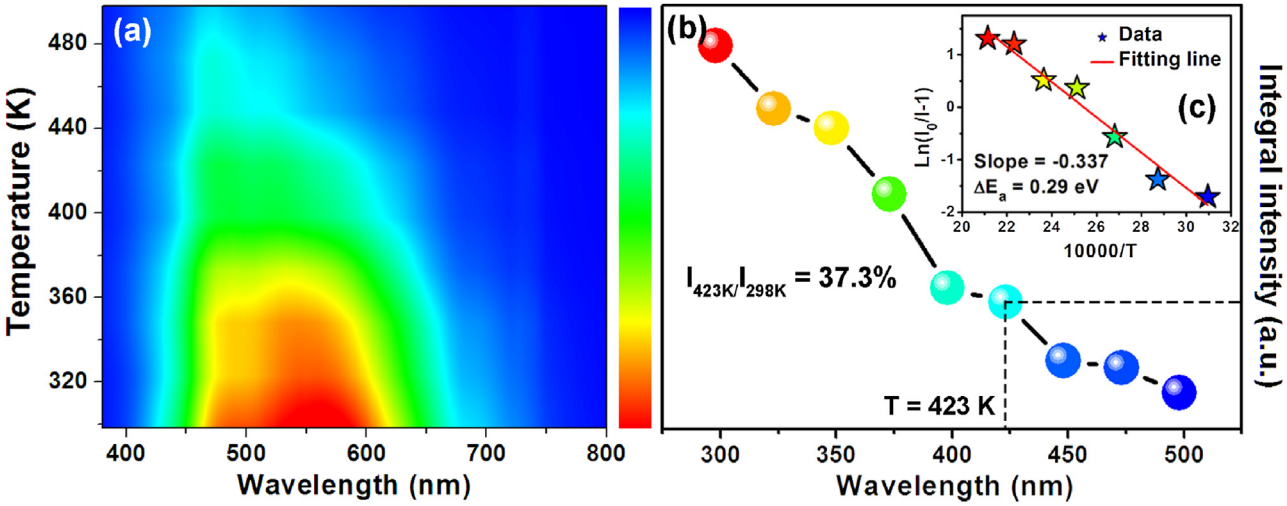

Fig. 3. Intensity map of temperature-dependent PL spectra (a) and the corresponding normalized the integrated (400–800 nm) intensity (b) as well as the plot of ln($I_0/I - 1$) *vs* 10000/T (c) for sample BGNPF: 0.9% Eu^{2+}.

shift with heating from 298 to 498 K, which is due to the thermally active phonon-assisted tunneling from the excited states of the low-energy emission band to those of the higher energy emission band. With the temperature increase, the probability of this effect continuously enhanced and the emission energy become higher and higher, which is reflected in the blue shift of temperature-dependence spectra [30].

The energy transfer of $Eu^{2+} \rightarrow Pr^{3+}$ in BGNPF: Eu^{2+}, Pr^{3+} phosphor

NIR light not only could indirectly promote the plant growth, but also could enhance the nutriments in food, which is as indispensable as blue and red light. The emission of Pr^{3+} covers the blue, red and NIR region, which is an important activator for plant growth phosphor. However, the narrow absorption cross-section of Pr^{3+} from the spin-forbidden *f–f* transitions leads to its low efficiency, which can be greatly enhanced through the introduction of efficient sensitizer. Generally, the significant overlap between the emission spectrum of sensitizer and the excitation of Pr^{3+} is necessary. The PLE and PL spectra of Eu^{2+} and Pr^{3+} solely doped BGNPF are shown in Fig. 4a and b , respectively. A strong and broad absorption belonging to the $4f^7 \rightarrow 4f^6 5d^1$ transition of Eu^{2+} and emission band ranging from 400 to 800 nm from Eu^{2+} were observed in BGNPF: Eu^{2+} (in Fig. 4a); whereas the excitation spectrum of BGNPF: Pr^{3+} consists of several absorption lines at 447, 470, and 484 nm from the ground level $^3H_4$ to $^3P_2$, $^3P_1$ and $^3P_0$ levels transitions of Pr^{3+} ion, and the PL spectrum includes strong red and NIR emission. Comparing Fig. 4a and b, an obvious overlap between the PL spectra of Eu^{2+} and the PLE spectra of Pr^{3+} was observed, which indicate that the efficient energy transfer from Eu^{2+} to Pr^{3+} is expected to occur in the Eu^{2+}–Pr^{3+} co-doped BGNPF.

The PLE and PL spectra of BGNPF: 0.9% Eu^{2+}, 1% Pr^{3+} phosphor are shown in Fig. 4c. The PLE spectra monitored at 570 nm (Eu^{2+}: $4f^6 5d^1 \rightarrow 4f^7$) and 1022 nm ($Pr^{3+}$: $^1G_4 \rightarrow {}^3H_4$) are similar except a group of sharp absorption lines from Pr^{3+} in the latter, but they all include the typical broad band (250–450 nm) absorption from Eu^{2+},

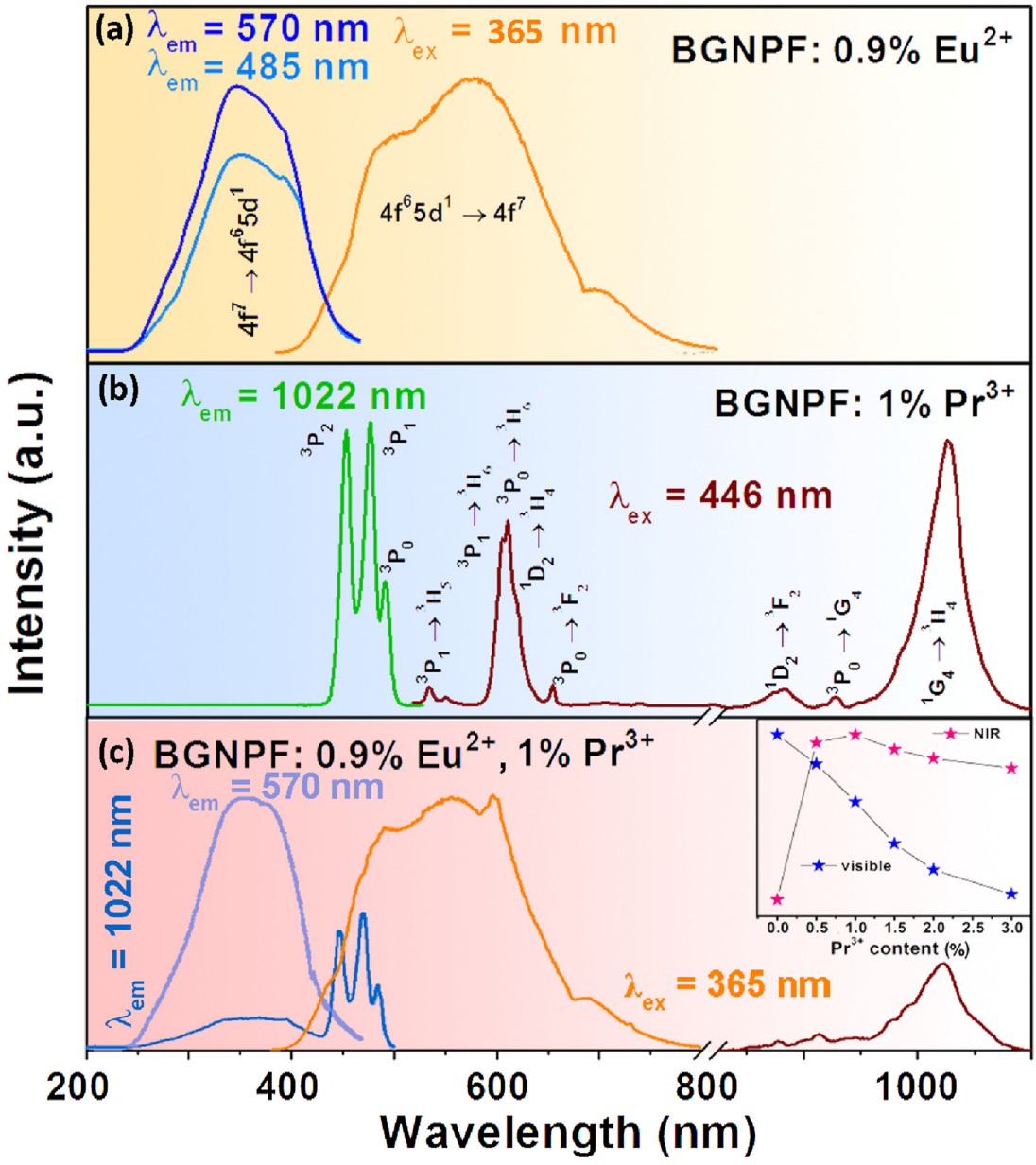

Fig. 4. The PLE and PL spectra of (a) BGNPF: 0.9% Eu^{2+}, (b) BGNPF: 1% Pr^{3+} and (c) BGNPF: 0.9% Eu^{2+}, 1% Pr^{3+}.Inset is the Pr^{3+} contents-dependent integral intensity of BGNPF: 0.9% Eu^{2+}, *y*Pr^{3+} samples in visible and NIR region.

which further confirm the occurrence of the energy transfer from Eu^{2+} to Pr^{3+} ions. Under the 365 nm excitation, the PL spectrum of phosphor BGNPF: 0.9 % Eu^{2+}, 1% Pr^{3+} composes of a broad emission band in visible region and a group of sharp emission lines peaked at 601 and 1022 nm from Eu^{2+} and Pr^{3+}, respectively. The integrated emission intensity in visible and NIR region of samples BGNPF: 0.9% Eu^{2+}, yPr^{3+} is offered as a function of Pr^{3+} concentration in the range of 0.5–3.0% in the inset of Fig. 4c. The visible emission intensity monotonously decreases whereas the NIR emission intensity first goes up and then declines with the increase of Pr^{3+} concentration due to the energy transfer from Eu^{2+} to Pr^{3+} and concentration quenching effect [31]. It is found that the emission spectra of BGNPF: Eu^{2+}, Pr^{3+} cover blue, red and NIR region, which match well with the absorption spectra of carotenoid, chlorophyll a, b and bacteriochlorophyll and imply that the prepared phosphor can be used in the plant growth LEDs.

To further testify the ET process from Eu^{2+} to Pr^{3+} ions in BGNPF: Eu^{2+}, Pr^{3+}, the decay curves and corresponding lifetimes of Eu^{2+} in BGNPF: 0.9%Eu^{2+}, yPr^{3+} phosphors (monitored at 485 nm) are exhibited in Fig. 5a. The decay curves can be well fitted by a second-order exponential using the following equations [32,33]:

$$I_\tau = I_0 + A_1 \exp\left(-\frac{t}{\tau_1}\right) + A_2 \exp\left(-\frac{t}{\tau_2}\right) \quad (5)$$

$$\tau^* = \frac{A_1\tau_1^2 + A_2\tau_2^2}{A_1\tau_1 + A_2\tau_2} \quad (6)$$

where I_t and I_0 are the luminescence intensities as time are 0 and t, A_1 and A_2 are constants, τ_1 and τ_2 are the fast and slow lifetimes, respectively, and τ^* is the effective lifetime. According to the Eqs. (5) and (6), τ^* is equal to about 448, 445, 382, 371, and 298 ns for y = 0.0%, 0.5%, 1.0%, 1.5%, and 2.0%, respectively. Obviously, the lifetimes of Eu^{2+} ions gradually decrease with the increase of Pr^{3+} concentration (as shown in Fig. 5b), which can further confirm the existence of energy transfer from Eu^{2+} to Pr^{3+} ions. The efficiency (η_τ) of energy transfer from Eu^{2+} to Pr^{3+} ions in the BGNPF: Eu^{2+}, Pr^{3+} is calculated according to the life time of Eu^{2+} based on the following equation [34]:

$$\eta_\tau = 1 - \frac{\tau}{\tau_0} \quad (7)$$

where τ_0 and τ stand for the decay lifetimes of the samples without and with the Pr^{3+} ions, respectively. The τ and η_τ are plotted as a function of the Pr^{3+} concentration in Fig. 5c, in which the ET efficiency from Eu^{2+} to Pr^{3+} increases gradually with the growth of Pr^{3+} concentration.

To further explain the energy transfer process, the energy level schematic diagram is depicted in Fig. 6. When excited at 220–450 nm, the electrons in the *4f* ground state can be pumped to the *5d* excited state, and then relaxed to the lowest excited state through non-radiative relaxation. There are two ways for Eu^{2+} ions to transfer their absorbed energy to Pr^{3+} ions, one is when the excited electrons go back partly to the ground state *4f* and give a broadband emission centered at 485 nm, then the emitted energy is partly reabsorbed by Pr^{3+} to pump the electrons from $^3H_4$ to $^3P_{0,\,1,\,2}$. The other energy transfer process works when a part of electrons at the excited *5d* level of Eu^{2+} directly transfer to the neighbor Pr^{3+} ions due to their close excited energy levels. Therefore, the energy transfer from Eu^{2+} to Pr^{3+} is the main pathway to populate the excited states $^3P_{0,\,1,\,2}$ and $^1I_6$ levels of Pr^{3+}. Then, the electrons at $^3P_2$ level non-radiative relax to the lower $^3P_1$ and $^3P_0$ levels, resulting in visible emission peaks at 526 ($^3P_1 \rightarrow {}^3H_5$), 596 ($^3P_1 \rightarrow {}^3H_6$), 601 ($^1D_2 \rightarrow {}^3H_4$), 610 ($^3P_1 \rightarrow {}^3H_6$) and 644 ($^3P_0 \rightarrow {}^3F_2$) nm [35]. In addition, phonon-assisted non-radiative relaxation (NR) from $^3P_0$ to $^1D_2$ level and cross-relaxation (CR) CR1 ($^3P_0 + {}^3H_6 \rightarrow {}^3H_4 + {}^1D_2$) and CR2 ($^3P_0 + {}^1D_2 \rightarrow {}^3H_4 + {}^3H_6$) also participate at high concentration and result in concentration quenching process. The energy gap between $^3P_0$ and $^1D_2$ is 3866 cm^{-1} and the maximum vibrational frequency of phosphate is 1037 cm^{-1}, so the non-radiation (NR) process may come up with 3–4 phonons assistance [32]. Therefore, the CR process plays an more important role in populating electrons to $^1D_2$ energy level than that of NR process, so the red emission at 601 nm ($^1D_2 \rightarrow {}^3H_4$) and NIR emission 865 nm ($^1D_2 \rightarrow {}^3F_2$) are relatively stronger. At the same time, the electrons will populate to the $^1G_4$ energy level through CR3 ($^1D_2 + {}^1G_4 \rightarrow {}^3H_4 + {}^3F_4$), then, a radiative transition to the ground state $^3H_4$ with 1022 nm ($^1G_4 \rightarrow {}^3H_4$) NIR emission take place. Furthermore, when electrons were populated to the $^3P_0$ energy level, the NIR two photon emissions ($^3P_0 \rightarrow {}^1G_4 \rightarrow {}^3H_4$) may occur by assimilating a visible photon and emitting two NIR photons, so the 916 ($^3P_0 \rightarrow {}^1G_4$) and 1022 ($^1G_4 \rightarrow {}^3H_4$) nm NIR light can be observed in the test [36]. Just as shown in Fig. 2b, the intensity of the peak at 916 nm is incredibly weaker than that of 1022 nm, which indicates

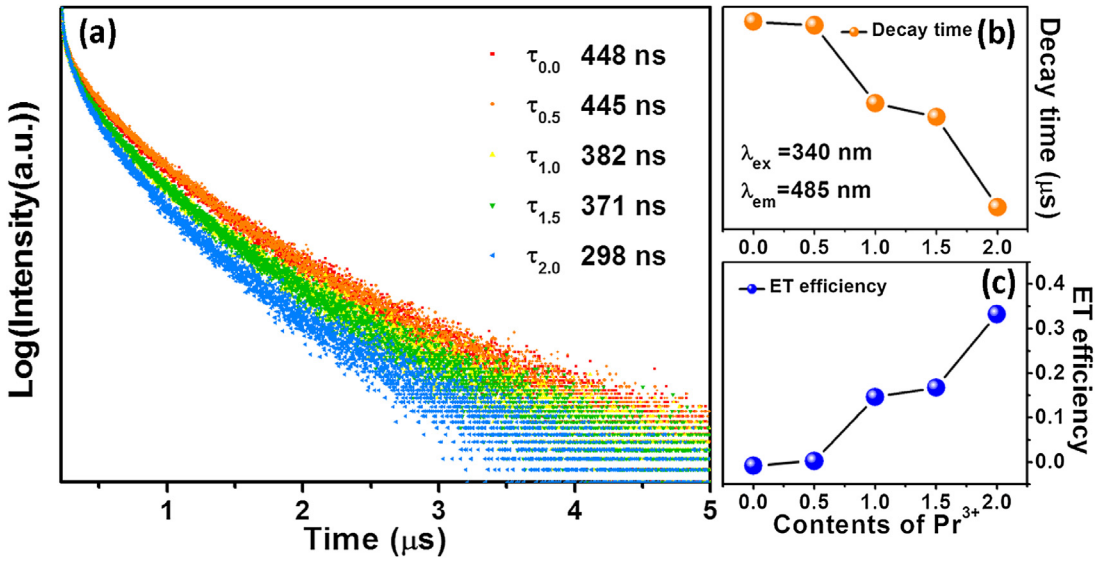

Fig. 5. (a) The decay curves, (b) decay time of Eu^{2+} and (c) energy transfer efficiency from Eu^{2+} to Pr^{3+} in phosphor BGNPF: 0.9% Eu^{2+}, yPr^{3+}as function of Pr^{3+} concentration.

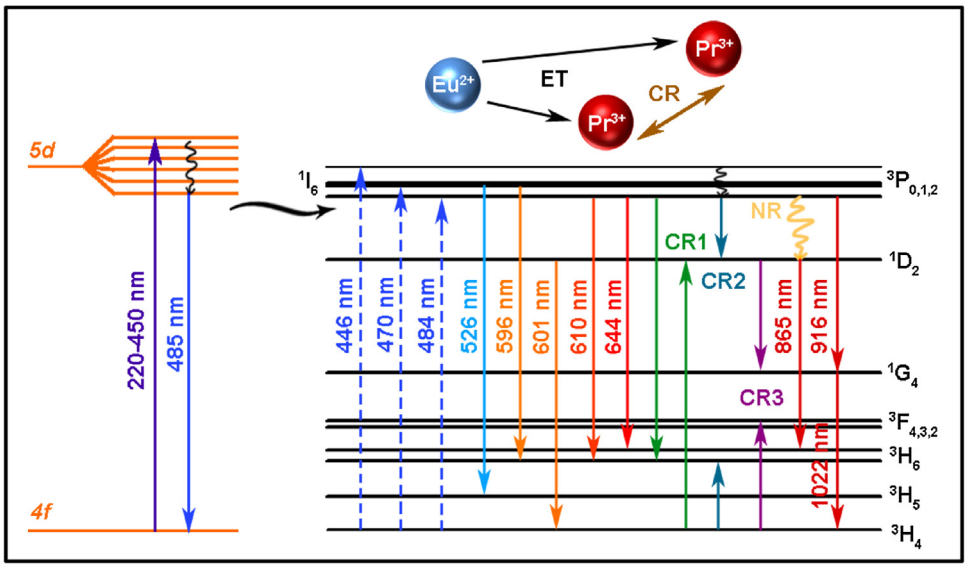

Fig. 6. Schematic energy level diagram and the energy transfer process among Eu^{2+} and Pr^{3+}.

that the possible of NIR two photon emissions is very slim. Therefore, the NIR emission is a closely linked CR/NR process.

Conclusion

In summary, a series of Eu^{2+}–Pr^{3+} co-doped apatite phosphors $Ba_4Gd_3Na_3(PO_4)_6F_2$: Eu^{2+}, Pr^{3+} used for plant growth LEDs were successfully synthesized by the traditional high-temperature solid-state method in a reduced atmosphere. The crystal structure of host $Ba_4Gd_3Na_3(PO_4)_6F_2$ was determined through the XRD refinement, in which three crystallographic sites were offered for Eu^{2+} possible occupancy. The assignment of three broad emission bands at 446, 484 and 593 nm to Eu^{2+} at the sites of Ba, Gd (1) (coordinated with 7O and 2F) and Gd (2) site (coordinated with 9O) was carried out through analysis of the liquid helium temperature photoluminescence spectra. The energy transfer processes from Eu^{2+} to Pr^{3+} were confirmed through the overlap of PL spectrum of BGNPF: Eu^{2+} and PLE spectrum of BGNPF: Pr^{3+} and the decrease of Eu^{2+} average lifetime in BGNPF: Eu^{2+}, Pr^{3+} with raising the concentration of Pr^{3+}. The evaluated sample BGNPF: Eu^{2+}, Pr^{3+} not only offers a strong and broad absorption band ranging from 220 to 420 nm, but also exhibits blue, red and NIR emissions, which implies that the emission spectra of the sample match well with the absorption spectra of pigments carotenoids, chlorophyll a, b and bacteriochlorophyll in plant with the excitation of n-UV light. Results indicate that the present phosphor BGNPF: Eu^{2+}, Pr^{3+} shows great potential for plant growth LEDs.

Acknowledgments

This work was supported by National Natural Science Foundation of China (No. 11704312, 11274251), Research Fund for the Doctoral Program of Higher Education of China (RFDP) (No.20136101110017), Foundation of Key Laboratory of Photoelectric Technology in Shaanxi Province (15JS101).

References

[1] C.C. Lin, A. Meijerink, R.S. Liu, J. Phys. Chem. Lett. 7 (2016) 495.
[2] Z.W. Zhou, J.M. Zheng, R. Shi, N.M. Zhang, J.Y. Chen, R.Y. Zhang, H. Suo, E.M. Goldys, C.F. Guo, ACS Appl. Mater. Interfaces 9 (2017) 6177.
[3] J.Y. Chen, N.M. Zhang, C.F. Guo, F.J. Pan, X.J. Zhou, H. Suo, X.Q. Zhao, E.M. Golys, ACS Appl. Mater. Interfaces 8 (2016) 20856.
[4] N. Yeh, J.P. Chung, Renew. Sustain. Energy Rev. 13 (2009) 2175.
[5] F. Valladares, A mechanistic view of the capacity of forests to cope with climate change, Managing Forest Ecosystems: The Challenge of Climate Change, Springer-Verlag Berlin and Heidelberg, Cham, 2017.
[6] Y.J. Yun, J.K. Kim, J.Y. Ju, S.K. Choi, W.I. Park, J.Y. Suh, H. Jung, Y. Kim, S. Choi, Phys. Chem. Chem. Phys. 19 (2017) 11111.
[7] Z.Y. Mao, J.J. Chen, D.J. Wang, Chem. Eng. J. 284 (2016) 1003.
[8] G.D. Massa, H.H. Kim, R.M. Wheeler, C.A. Mitchell, Hortscience 43 (2008) 1951.
[9] M.M. Shang, C.X. Li, J. Lin, Chem. Soc. Rev. 43 (2014) 1372.
[10] C.F. Guo, H. Suo, Design of single-phased multicolor-emission phosphor for LED phosphors, Up Conversion Nano Particles, Quantum Dots and Their Applications, Springer-Verlag Berlin and Heidelberg, Cham, 2017.
[11] M.M. Shang, S.S. Liang, N.R. Qu, H.Z. Lian, J. Lin, Chem. Mater. 29 (2017) 1813.
[12] Z.G. Xia, Y.Y. Zhang, M.S. Molokeev, V.V. Atuchin, J. Phys. Chem. C 117 (2013) 20847.
[13] Z.G. Xia, Y.Y. Zhang, M.S. Molokeev, V.V. Atuchin, Y. Luo, Sci. Rep. 3 (1–7) (2013) 3310.
[14] H.P. Ji, Z.H. Huang, Z.G. Xia, M.S. Molokeev, V.V. Atuchin, M.H. Fang, Y.G. Liu, J. Phys. Chem. C 119 (2015) 2038.
[15] W.J. Zhou, F.J. Pan, L. Zhou, D.J. Hou, Y. Huang, Y. Tao, H.B. Liang, Inorg. Chem. 55 (2016) 10415.
[16] X.P. Fu, W. Lü, M.M. Jiao, H.P. You, Inorg. Chem. 55 (2016) 6107.
[17] A. Huang, Z.W. Yang, C.Y. Yu, Z.H. Chai, J.B. Qiu, Z.G. Song, J. Phys. Chem. C 121 (2017) 5267.
[18] Bruker AXS TOPAS V4: General Profile and Structure Analysis Software for Powder Diffraction data. User's Manual, Bruker AXS, Karlsruhe, Germany, 2008.
[19] M. Mathew, I. Mayer, B. Dickens, L.W. Schroeder, J. Solid State Chem. 28 (1979) 79.
[20] Y.C. Wang, J.Y. Ding, Y.Y. Li, X. Ding, Y.H. Wang, Chem. Eng. J. 315 (2017) 382.
[21] L.G. Van Uitert, J. Lumin. 29 (1984) 1.
[22] L. Wang, R.J. Xie, T. Suehiro, T. Takeda, N. Hirosaki, Chem. Rev. 118 (2018) 1951.
[23] J.M. Wang, H. Lin, Q.M. Huang, G.C. Xiao, J. Xu, B. Wang, T. Hu, Y.S. Wang, J. Mater. Chem. C 5 (2017) 1789.
[24] Q. Zhang, X.C. Wang, X. Ding, Y.H. Wang, Dyes Pigm. 149 (2018) 268.
[25] S.P. Lee, T.S. Chan, T.M. Chen, ACS Appl. Mater. Interfaces 7 (2015) 40.
[26] W.Z. Sun, Y.L. Jia, R. Pang, H.F. Li, T.F. Ma, D. Li, J.P. Fu, S. Zhang, L.H. Jiang, C.Y. Li, ACS Appl. Mater. Interfaces 7 (2015) 25219.
[27] L.G. Van Uitert, J. Electrochem. Soc. 114 (1967) 1048.
[28] X.Y. Liu, H. Guo, Y. Liu, S. Ye, M.Y. Peng, Q.Y. Zhang, J. Mater. Chem. C 4 (2016) 2506.
[29] P.P. Dai, C. Li, X.T. Zhang, J. Xu, X. Chen, X.L. Wang, Y. Jia, X.J. Wang, Y.C. Liu, Light: Sci. Appl. 5 (2016)e16024.
[30] Z.Y. Zhao, Z.G. Yang, Y.R. Shi, C. Wang, B.T. Liu, G. Zhu, Y.H. Wang, J. Mater. Chem. C 1 (2013) 1407.
[31] H.J. Guo, Y.H. Wang, G. Li, J. Liu, P. Feng, D.W. Liu, J. Mater. Chem. C 5 (2017) 2844.
[32] J.Y. Chen, C.F. Guo, Z. Yang, T. Li, J. Zhao, J. Am. Ceram. Soc. 99 (2016) 218.
[33] H. Suo, C.F. Guo, T. Li, J. Phys. Chem. C 120 (2016) 2914.
[34] P.L. Li, Z.J. Wang, Z.P. Yang, Q.L. Guo, J. Mater. Chem. C 2 (2014) 7823.
[35] W.B. Dai, Y.F. Lei, J. Zhou, M. Xu, L.L. Chu, L. Li, P. Zhao, Z.H. Zhang, J. Alloys Compd. 726 (2017) 230.
[36] Y. Chen, J. Wang, C.M. Liu, J.K. Tang, X.J. Kuang, M.M. Wu, Q. Su, Opt. Express 21 (2013) 3161.